THE JOURNAL OF PHYSICAL CHEMISTRY C
A JOURNAL OF THE AMERICAN CHEMICAL SOCIETY

pubs.acs.org/JPCC

Article

Mechanisms of Acoustic Desorption of Atomic Clusters and Exfoliation of Graphene Multilayers

Maxim V. Shugaev and Leonid V. Zhigilei*

Cite This: J. Phys. Chem. C 2021, 125, 23313–23326

Read Online

ACCESS | Metrics & More | Article Recommendations

ABSTRACT: The phenomenon of acoustic desorption is studied in a series of atomistic simulations that account for the nonlinear evolution of the acoustic wave profiles during the wave propagation through the substrates. The simulations performed for atomic clusters demonstrate a nonthermal nature of the desorption from surfaces exposed to the acoustic waves. The acoustic desorption is characterized by a sharp threshold-like dependence of the desorption probability on the binding energy of the adsorbates and a nearly linear increase of the threshold binding energy for the desorption on the mass of the adsorbates. The equivalent temperature required for reproducing the acoustic desorption through the thermal activation is estimated to be more than 20 times higher than the actual substrate temperature. The extension of the investigation to the acoustic exfoliation of graphene multilayers from Cu(111) substrate demonstrates the ability of strong nonlinear acoustic pulses to cause the ejection of multilayers of various thicknesses while keeping a single graphene layer on the substrate. For both the atomic clusters and thin graphene multilayers, the nonlinear sharpening of the acoustic waves during their propagation through the substrates plays a key role in creating the conditions for acoustic desorption/exfoliation. A simple analytical model based on the consideration of resonant coupling of high-frequency harmonics of the nonlinear acoustic waves with the vibrational modes of the adsorbates is formulated and is shown to provide a reliable semiquantitative estimate of the conditions for the desorption of atomic clusters and thin graphene multilayers. For a thicker graphite overlayer, with a thickness exceeding that of the shock front of the wave, the acoustically driven ejection (or spallation) of the overlayer is described at the continuum level, by considering the reflection, transmission, and interaction of stress waves in the surface region of the system. The computational predictions have practical implications for interpretation of the results of laser-induced acoustic desorption mass spectrometry experiments and provide ideas for the development of new approaches utilizing the acoustic energy in thin film growth, transfer of 2D materials, and regeneration of the catalytic activity of metal surfaces.

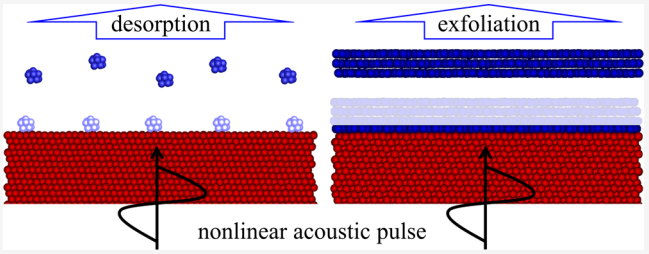

1. INTRODUCTION

Acoustic desorption is a process where the interaction of acoustic waves with surfaces causes the ejection/desorption of atoms, molecules, or atomic clusters.[1−25] First reported as a scientific curiosity,[1,2] this process has been recognized as a useful tool for the acoustic control of surface reactions and catalytic activity of surfaces,[4−7] as well as for "cold" desorption of heat-sensitive organic molecules for mass spectrometry analysis.[8−25] The mass spectrometry applications of the acoustic desorption commonly rely on the ability of short laser pulses to generate strong acoustic waves in irradiated targets[26,27] and are often referred to as laser-induced acoustic desorption (LIAD).

In its simplest form, LIAD has a layout where the molecules of interest (analytes) are deposited on the front side of a thin metal foil facing the mass spectrometer, while the laser irradiates the back side of the film launching an acoustic pulse toward the front surface and leading to the desorption of the analytes.[9,12−25] Placing the irradiated side of the metal foil in direct contact with an optically transparent solid substrate of liquid layer has been shown to increase the efficiency of acoustic desorption,[18,19] which can be attributed to higher amplitudes of compressive pressure pulses generated under conditions of spatial confinement in both ablative and nonablative irradiation conditions.[28−30] An alternative setup, where an absorbing metal layer (liquid mercury) is confined between two sapphire plates, has also been demonstrated to be effective for the generation of strong acoustic pulses leading to desorption of electrons, ions, and molecules.[10,11] Note that, while metal foils are used most commonly for the generation

Received: August 17, 2021
Revised: September 22, 2021
Published: October 14, 2021

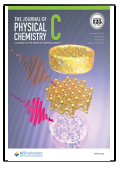

and transmission of acoustic pulses in LIAD, the acoustic desorption has also been reported from a Si substrate[31] and the molecular sample itself.[8]

The practical relevance of LIAD, capable of volatilization of intact, thermally labile molecules with very limited excitation of intramolecular vibrational states,[8,12,19] has attracted substantial interest from the mass spectrometry community and induced active discussions of the underlying mechanisms. A qualitative "shake-off" desorption mechanism, ascribing the molecular ejection to the sudden displacement of the front surface of the irradiated substrate caused by the laser-generated pressure wave, has been proposed in the first studies of LIAD.[8,9] It has been later suggested that the surface velocity v required for the desorption through the shake-off mechanism should exceed a minimum level that can be expressed as $v_{min} = \sqrt{2E_b/M}$, where E_b and M are the binding energy and mass of the surface species, respectively.[14] The assumption behind this simple relation is that the surface velocity increases instantaneously from zero to v upon the arrival of the wave to the surface, while the surface species do not move during this surface acceleration. As a result, the surface species acquire a relative velocity of v toward the surface in the surface frame of reference. Further assuming that no energy redistribution into internal degrees of freedom occurs during the "collision" of the surface species with the surface, the maximum velocity of the surface species away from the surface is v, and the shake-off criterion of $v > v_{min}$ is simply stating that the kinetic energy of the surface species in the surface frame of reference should be larger than their binding energy. Despite the rather strong simplifications of this analysis, i.e., the assumptions of the instantaneous surface velocity change and the absence of the energy transfer to internal degrees of freedom upon the desorption, it still provides a simple lower bound estimate of the surface velocity required for the desorption of particular species.

The analogy between LIAD and photomechanical spallation has also been drawn in the literature,[9,10] and the need for the resonance conditions between the acoustic excitation and the frequencies of the adsorbate−surface bonds has been pointed out.[11] The attempts of quantitative mapping of the LIAD conditions to the requirements of the shake-off model, however, reveal some difficulties. In particular, the large mismatch between the relatively low frequencies of the acoustic waves generated in LIAD experiments, typically below a few hundred megahertz for nanosecond laser pulses,[26] and the vibrational frequencies characteristic of atoms and molecules on the surface, on the order of terahertz, calls into question the possibility of the direct resonant coupling of the acoustic wave to surface vibrational states[11,32,33] and the validity of the shake-off criterion that assumes an instantaneous change of the surface velocity.[14]

The perceived implausibility of the direct dynamic coupling of acoustic waves to surface species gives impetus for a search for alternative mechanisms. In particular, a transient modification of the binding energies and diffusion barriers of adsorbed species induced by the surface strain[34−36] has been considered as a possible mechanism that may be responsible for the acoustic activation of surface diffusion[37] and desorption.[3,36] The results of atomistic modeling,[37] however, suggest that, at realistic levels of surface strain caused by acoustic waves, the modification of the energy barriers is not sufficient to have any significant effect on the rates of surface processes. An alternative hypothesis based on the presumed presence of mesoscopic surface structures/domains that can effectively couple to a long-wavelength acoustic excitation has been suggested to explain the acoustic enhancement of chemical reactions on catalytic surfaces.[38,39] A similar idea of the presence of strained molecular islands or continuous films formed in the process of drying of analyte solutions on LIAD substrates/foils was proposed in ref 14. The strained surface features are then assumed to release the stored elastic energy in response to an acoustic stimulus, thus providing the needed extra energy for the desorption of molecules in LIAD. Although the latter idea has received a wide acceptance in the LIAD community,[16,19,21−25] we note that the connection between the release of the elastic energy stored in the strained films/islands and the desorption of intact molecular analytes has been demonstrated neither experimentally nor computationally so far.

The absence of the unifying physical picture of acoustic desorption can largely be attributed to two main factors. The first factor is the diverse range of experimental setups used in LIAD studies, which makes it difficult to expect that a single physical mechanism would be responsible for the acoustically induced desorption in all cases. The thickness and type of the substrate define the generation[13,19] and evolution (nonlinear sharpening and dissipation)[40−42] of the acoustic waves, as well as the possible contribution of thermal desorption due to the heat transfer from the irradiated back side to the front side of the substrate.[8,9] In particular, while a slow increase in the molecular signal on the time scale of ∼10 μs is interpreted in ref 23 as evidence in favor of the stored-surface-strain desorption model,[14] this time scale exceeds the characteristic time of the heat diffusion through the 10 μm thick tantalum foil used in this study, suggesting a possible contribution of the thermal desorption. Furthermore, the analyte samples in LIAD experiments also exhibit a large variation of thickness, from micrometers[13,15] to about a monolayer coverage[14] and to individual atomic or molecular adsorbates present on bare metal surfaces.[10,11] The mechanism of the acoustic desorption from a bare surface is likely to be rather different from that from a micrometer-thick molecular layer. Beyond the variability of experimental setups in LIAD studies, the second major factor explaining the limited mechanistic understanding of acoustic desorption is the virtual absence of experimental and computational efforts focused specifically on revealing the molecular-level processes leading to the molecular ejection in LIAD.

In this paper, we investigate the mechanisms of acoustic desorption based on the results of atomistic molecular dynamics (MD) simulations performed for two model systems: a generic model of small atomic clusters deposited on a substrate and a model representing graphene single layers and multilayers grown on Cu(111) surface. At the qualitative level, the conditions leading to the acoustic desorption in the simulations of the two model systems can be related to the LIAD setups with submonolayer analyte coverage and a continuous analyte sample layer, respectively. In both cases, we find that the nonlinear sharpening of strong laser-generated acoustic waves during their propagation through the substrates plays a key role in creating the conditions for the desorption of atomic clusters and thin graphene multilayers. For the atomic clusters, the nonlinear sharpening of a wave is associated with the generation of high-frequency harmonics, which can reach the resonance frequencies of the adsorbates and can lead to an

https://doi.org/10.1021/acs.jpcc.1c07311
J. Phys. Chem. C 2021, 125, 23313−23326

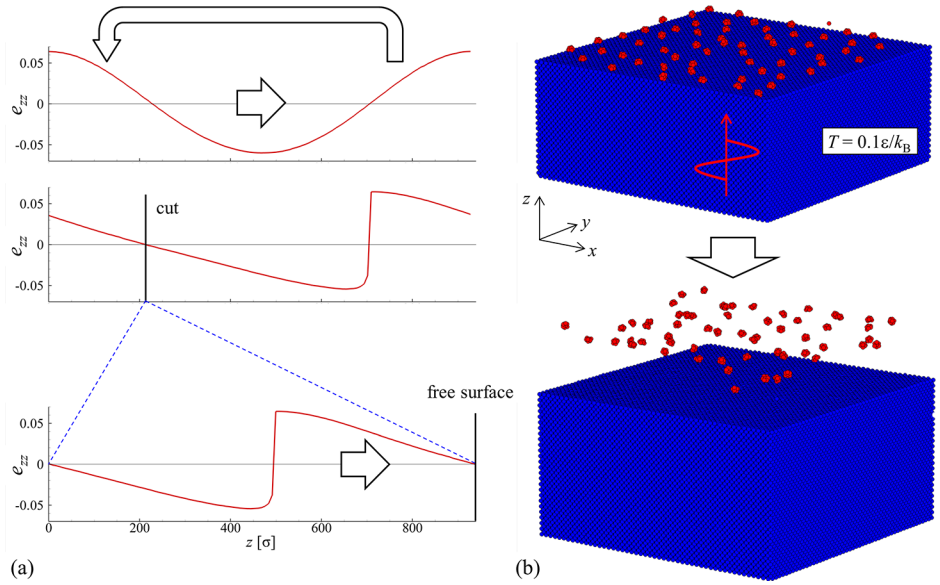

Figure 1. Schematic illustration of the computational setup used for simulation of acoustic desorption of atomic clusters. (a) First, the evolution of the wave profile during the nonlinear propagation of the wave in the substrate is simulated in a system with periodic boundary condition applied in the direction of the wave propagation. After a shock front is formed (middle panel), the system is split at a position of zero strain (bottom panel), and atomic clusters are placed and relaxed on the newly formed surfaces. (b) The simulation is then continued, and the clusters are desorbed as a result of the reflection of the wave from the surface, as illustrated by snapshots of a surface region of the substrate. The atoms in the substrate and clusters are colored blue and red, respectively.

effective dynamic coupling between the acoustic wave and the surface vibrational modes. For the graphene multilayers that are thicker than the thickness of the shock front, the ejection of a multilayer from the substrate can be described in terms of the partial transmission of the acoustic wave into the multilayer, reflection of the transmitted wave from the free surface, and the interaction of the reflected and incident waves leading to the mechanical spallation and ejection of the overlayer from the substrate. A simplified analytical model accounting for the need for the resonance conditions in LIAD is formulated based on the computational results and is shown to provide a uniform description of the desorption of small atomic clusters as well as the acoustic exfoliation of multilayer graphene from a Cu catalytic substrate. A description of the computational models is provided in section 2 and is followed by the presentation and discussion of computational results on the acoustically activated desorption of small clusters in section 3 and the ejection/exfoliation of graphene in section 4. A summary of the results is provided in section 5.

2. COMPUTATIONAL MODELS

2.1. Generation and Nonlinear Propagation of Acoustic Waves. The direct MD simulation of the laser-induced generation of a strong acoustic wave followed by its propagation through the substrate requires an excessively large computational system and is computationally expensive. At the same time, as evidenced by the results presented in sections 3 and 4, the nonlinear sharpening of the acoustic waves in the course of their propagation through the substrate plays a critical role in the desorption process. Thus, to simulate the evolution of an acoustic wave profile during its free propagation through a substrate, we use the computational "synchrotron" approach recently developed for atomistic simulations of nonlinear acoustic waves.[42]

Within this approach adapted for a plane longitudinal wave propagating through the substrate along the z-axis, a harmonic (sinusoidal) wave is introduced into an initial thermally equilibrated system by adding extra displacements and velocities to atoms in the direction of wave propagation according to $\Delta z = A \sin(kz_i^0)$ and $\Delta v_z = Akc \cos(kz_i^0)$, where $k = 2\pi/\lambda$ is the spatial angular frequency (wavenumber), λ is the wavelength, c is the speed of the wave (speed of sound in the direction of the wave propagation), z_i^0 is the z coordinate of an atom i in the initially generated system (accounting for the thermal expansion), and A is the wave amplitude set to reproduce a particular initial strain amplitude that is calculated as $e_0 = Ak$. The size of the system in the direction of the wave propagation, L_z, is chosen to be equal to the wavelength of the initial wave, i.e., $\lambda = L_z$.

As schematically shown in the top frame of Figure 1a, the generation of the initial wave is followed by the simulation of a free circulation of the wave within the system, with periodic boundary conditions applied in all directions, including the direction of the wave propagation. While the wave is circulating within the computational system, the increasing time in the simulation can be related to the time of the wave propagation from the source near the irradiated back surface of the substrate toward the front surface. Due to the nonlinearity of the elastic properties of the substrate material, the wave profile undergoes a nonlinear sharpening and formation of a shock front, as illustrated in Figure 1a. At a particular moment, defined as a time when the wave is approaching the surface of the substrate, the system is cut at the position of zero strain to form two free surfaces, and the periodic boundary condition along the direction of the wave propagation is removed. The fully relaxed adsorbates or a graphene overlayer are then added to the front surface and subjected to the energy minimization procedure (quenching) to ensure that the structures added to the surface do not have any excess energy that may contribute to their desorption. Note that the quenching is only applied to the surface structures, while all the atoms in the substrate maintain the instantaneous positions and velocities they have

https://doi.org/10.1021/acs.jpcc.1c07311
J. Phys. Chem. C 2021, 125, 23313−23326

at the time the free surfaces are introduced. After the relaxation of the surface structures, the MD simulation involving all atoms in the system is resumed, the wave moves toward the front surface and reflects from it, while the adsorbates or overlayers can be ejected/desorbed, as illustrated schematically for the acoustic desorption of atomic clusters in Figure 1b.

The parameters of the initial wave, i.e., e_0 and λ, are chosen to ensure that the process of the nonlinear sharpening of the wave profile and the acoustic desorption can be simulated at a reasonable computational cost. The distance that the initially sinusoidal wave has to travel in a material with nonlinear elastic properties before the shock front formation is directly proportional to the wavelength and inversely proportional to the initial strain magnitude of the wave.[40−42] To enable the exploration of the effect of the acoustic desorption within the relatively short time scale accessible to MD simulations, the values of the initial strain are chosen to be higher and the wavelengths are chosen to be shorter (see sections 3 and 4) than those usually realized in LIAD experiments. The longer paths of the waves propagating through the substrates in LIAD experiments (usually above 10 μm)[8−25] suggest that the wave profile sharpening, similar to that observed in the simulations, can be expected for weaker, lower frequency waves generated in the experiments.

2.2. Atomic Clusters on a Substrate. The general mechanisms of acoustic desorption are investigated with a model system consisting of a substrate with a face-centered cubic (fcc) structure and 10-atom clusters placed on the (001) surface of the substrate. The interatomic interactions are described by the Lennard-Jones (LJ) potential with parameters σ and ε, defining the length and energy scales of the substrate. A cutoff function[43] is used to ensure that the interactions vanish at a cutoff distance of 3σ. All the parameters of the computational setup and the quantities calculated in the simulations are expressed in units of LJ length and energy parameters, as well as the mass of an atom in the substrate, m. In particular, the unit of time is $\tau = (m\sigma^2/\varepsilon)^{1/2}$.

The dimensions of the substrate are $78\sigma \times 78\sigma \times 935\sigma$ (50 × 50 × 600 fcc unit cells), which corresponds to 6 million atoms. Before the introduction of the acoustic wave, the substrate is equilibrated at a temperature of $0.1\varepsilon/k_B$ (the equilibrium melting temperature of the model LJ material is $\sim 0.78\varepsilon/k_B$)[44] with periodic boundary conditions applied in all three directions. At this temperature, the speed of sound in the direction of the wave propagation, c, is equal to $9.23\sigma/\tau$. The thermally equilibrated system is then used in the simulation of the nonlinear propagation of an acoustic wave and its interaction with a free surface created as described in section 2.1.

After the free surface is introduced, about 60 10-atom clusters are randomly placed on the surface at a sufficient distance from each other ($\geq 5\sigma$), so that there is no direct interaction between the clusters. The interatomic interactions between atoms within a cluster are described by the LJ potential with parameters $\sigma_{cc} = 0.6\sigma$ and $\varepsilon_{cc} = 3.72\varepsilon$, chosen so that the 10-atom clusters retain their integrity during the desorption process. These parameters are the same as in the investigation of the enhancement of surface diffusion by surface acoustic waves reported in ref 45. The length parameter for the cluster−substrate interactions is $\sigma_{cs} = \sigma$, while ε_{cs} is varied to change the surface binding energy of the clusters, E_b, and to establish the dependence of the desorption probability on E_b. The mass of an atom in a cluster is $m_c = 1.74m$ in most of the simulations but is varied to explore the importance of the resonance conditions, as specified in the text. The simulations are performed with an in-house MD code earlier applied for simulations of acoustic activation of surface diffusion,[37,45] acoustically induced structuring of surface adatoms,[46] and nonlinear propagation of surface acoustic waves.[42]

2.3. Graphene Layers on Cu(111) Surface. Following the analysis of the general mechanisms of acoustic desorption performed for atomic clusters deposited on the LJ substrate, the simulations are extended to Cu substrates covered by single-layer and multilayer graphene. In addition to the exploration of an intriguing possibility of using the acoustic energy for exfoliation of graphene from a metal substrtate, this system may provide some general insights into the mechanisms involved in the molecular ejection from continuous layers of analyte samples commonly used in LIAD.[12,13,15−25] While the multilayer graphene is certainly not the most realistic representation of a molecular overlayer formed by drying an analyte solution, the relatively weak van der Waals nature of bonding between the graphene layers makes it possible to consider this system as a simplified one-dimensional analogue of an analyte sample.

The Cu substrate with (111) surface orientation is represented by a computational cell with dimensions of 2.2 nm × 2.1 nm × 207 nm consisting of 80 000 atoms. The bulk longitudinal waves are introduced into the system, and single-layer or multilayer graphene is added to the surface following the procedure described in section 2.1. The interactions between Cu atoms in the substrate are described by the embedded atom method (EAM) potential parametrized by Mishin.[47] The graphene is described with the adaptive intermolecular reactive empirical bond order (AIREBO) potential.[48] The van der Waals interaction between graphene and substrate is described by the LJ potential with σ = 3 Å and ε = 0.016 eV fitted in ref 49. This set of parameters is recommended in ref 49 because of its ability to realistically reproduce the experimentally observed Moiré superstructures. In our study, we use zero angle rotation of graphene when placing it on Cu, and the graphene is slightly stretched to match the periodic structure of the Cu(111) surface. The Cu−graphene interface binding energy calculated for this setup is equal to 117 meV/atom (here and below, the energy is given per area that corresponds to a C atom in a single graphene layer), which is close to the experimental value of 118 meV/atom (0.72 ± 0.07 J/m^2) determined for monolayer graphene synthesized on a copper substrate in nanoscale fracture mechanics measurements.[50] Meanwhile, *ab initio* density functional theory (DFT) calculations[51] performed for the most stable configuration of monolayer graphene on the Cu(111) surface predict a lower value of 65.1 meV/atom. For separation of a double-layer graphene from the Cu substrate, our model predicts a binding energy of 122 meV/atom, while the energy of separation of two freestanding graphene sheets from each other is 41.0 meV/atom. The simulations of acoustic exfoliation of graphene are performed with the LAMMPS software package.[52]

3. MECHANISMS OF ACOUSTIC DESORPTION OF SMALL CLUSTERS

In this section, we use the model system described in section 2.2 to investigate the general mechanisms of acoustic desorption of small atomic clusters. The simplicity of the

https://doi.org/10.1021/acs.jpcc.1c07311
J. Phys. Chem. C 2021, 125, 23313−23326

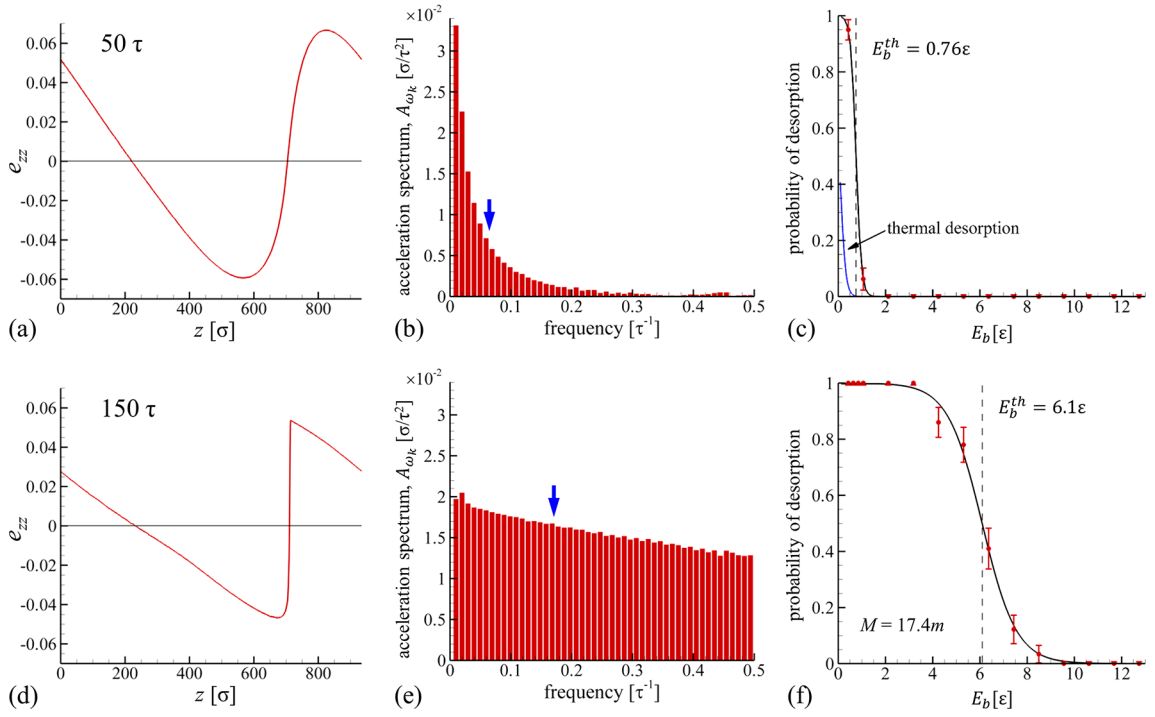

Figure 2. Wave profiles (a, d), corresponding spectra of the wave (b, e), and dependence of desorption probability on the cluster binding energy (c, f) for waves propagating for 50τ and 150τ before reaching the surface. The wave profiles and the corresponding spectra are obtained in a simulation with periodic boundary condition and exhibit the sharpness of the wave front expected at the moment of its reflection from the surface. The initial wave strain amplitude is 0.0628. Blue arrows in (b) and (e) mark the resonance frequency of a cluster on the surface recomputed for the binding energy of E_b^{th}, which corresponds to 0.5 probability of desorption for a particular wave. The amplitude of harmonics in the acceleration spectrum, A_{ω_k}, is calculated as explained in the text. The blue curve in (c) shows the probability of thermal desorption calculated using eqs 7 and 8.

model described by a relatively small number of parameters does not allow us to quantitatively represent any particular LIAD system, but the same simplicity enables a systematic variation of the key parameters affecting the acoustic desorption (e.g., surface binding energy and mass of the adsorbates) and facilitates a straightforward interpretation of simulation results. Moreover, the nonlinearity of the elastic properties of real materials is captured by the LJ potential,[42] making it possible to reproduce the nonlinear sharpening of the acoustic wave profiles and the resonant coupling of high-frequency harmonics of the nonlinear wave to the motion of surface adsorbates. The results of the MD simulations are related to predictions of a simplified analytical model, which is presented next, in section 3.1.

3.1. Analytical Model for Desorption Caused by a Nonlinear Acoustic Pulse. In order to provide a simplified analytical description of the acoustic desorption, an atomic cluster or a molecule adsorbed on a surface is treated as a harmonic oscillator with an effective mass M attached to the surface and characterized by a fixed angular frequency ω_0. The adsorbate is desorbed from the surface when the energy transferred to the oscillator exceeds the binding energy of the adsorbate, E_b. The total energy transferred to an oscillator due to the action of an arbitrary force $F(t)$ can be expressed as[53]

$$E = \left| \int_{-\infty}^{\infty} F(t) e^{-i\omega_0 t}\, dt \right|^2 /2M \tag{1}$$

Using the definition of the Fourier transform, one can rewrite eq 1 as $E = |\hat{F}(\omega_0)|^2/2M$, where $\hat{F}(\omega_0)$ is the amplitude of the Fourier transform of the external force at a frequency of ω_0. When the incoming acoustic wave is reflecting, the surface moves with an acceleration a. Therefore, in the frame of reference moving with the surface, the cluster experiences an inertial force of $F(t) = -Ma = -M\ddot{u}_{surf}$, where u_{surf} is the displacement of the surface. Using the formula for Fourier transform of derivatives, we can rewrite eq 1 as

$$E = \left|\hat{F}(\omega_0)\right|^2/2M = \left|\widehat{\ddot{u}_{surf}}(\omega_0)\right|^2 M/2 = \left|-\widehat{u_{surf}}(\omega_0)\,\omega_0{}^2\right|^2 M/2 \tag{2}$$

For a harmonic bulk wave, the displacement of the material in the substrate at a position z and time t can be described as $u_z(z,t) = A\sin(kz + \omega t + \varphi_0)$, where A, k, ω, and φ_0 are the amplitude, wavenumber, angular frequency, and phase of the wave. The strain can then be expressed as

$$e_{zz}(z,t) = \frac{\partial u_z(z,t)}{\partial z} = kA\cos(kz + \omega t + \varphi_0) = e_0\cos(kz + \omega t + \varphi_0) \tag{3}$$

where $e_0 = kA$ is the wave strain amplitude. The velocity within the wave can be expressed as

$$v_z(z,t) = \frac{\partial u_z(z,t)}{\partial t} = \omega A\cos(kz + \omega t + \varphi_0) = ce_0\cos(kz + \omega t + \varphi_0) \tag{4}$$

where $\omega = ck$. This expression also provides the maximum value of the material velocity produced by the wave with a strain amplitude of e_0:

$$v_{max} = ce_0 \tag{5}$$

When an initially harmonic wave propagates through a nonlinear medium, the wave profile can undergo sharpening and an eventual formation of a shock front. Such a wave may

https://doi.org/10.1021/acs.jpcc.1c07311
J. Phys. Chem. C 2021, 125, 23313−23326

be represented as a superposition of harmonic waves with different frequencies (multiple of the original frequency) propagating together. These waves are called high-frequency harmonics of the original wave. The Fourier transform can be used to decompose the wave profile into magnitudes of individual harmonics representing the wave. This procedure is illustrated in the left and middle panels of Figure 2 for the strain profiles of a wave sharpened by the propagation in the LJ crystal. The strain profile coincides with the velocity profile if multiplied by the speed of sound, similar to eq 5. Therefore, to get the spectrum of accelerations, used in eq 2 for evaluation of the energy transfer to the surface species, the results of the Fourier transform should be multiplied by $c\omega$. The results, shown in Figure 2 for two moments of time, 50τ and 150τ after the generation of an initially harmonic wave with a strain amplitude of 0.0628, illustrate the relation between the wave sharpening (left panels) and the evolution of the spectrum of accelerations (middle panels).

As explained in section 2.1, the initial propagation and nonlinear sharpening of the wave profile is simulated in a system with periodic boundary condition applied along the wave propagation direction. This allows us to apply the discrete Fourier transform for the calculation of the spectrum of the wave and to reduce the effect of thermal noise on the wave profile by averaging in a frame of reference moving with the wave. Once the wave profile acquires a desired shape, the acoustically induced desorption is simulated by introducing a free surface with adsorbates and exposing it to the nonlinear wave. Since the pulsed laser irradiation in LIAD produces an acoustic pulse rather than a continuous wave, only one period of the wave is considered in both MD simulations and the theoretical analysis. In particular, to represent the desorption by a single pulse, the integration in eq 1 should be done within the time interval from 0 to $T = \lambda/c$, rather than from $-\infty$ to ∞.

The external force acting on the adsorbates can be decomposed into components corresponding to different harmonics: $F(t) = -M\sum_k 2A_{\omega_k} \sin(\omega_k t)$, where ω_k and A_{ω_k} are the angular frequency and the amplitude of harmonic k in the acceleration spectrum discussed above. The amplitudes of the harmonics are multiplied by a factor of 2 since, in contrast to the free propagation of the wave, the interaction of the wave with a free surface involves a summation of the incident and reflected waves, making the displacement of the surface upon the wave reflection twice larger than the displacement in the bulk of the substrate caused by the propagating wave. During the integration of eq 1, all terms of the spectrum will give zero contribution except for the one with $\omega_k = \omega_0$ frequency:

$$E = \left|\int_0^T F(t)e^{-i\omega_0 t}\,dt\right|^2/2M = \left|\int_0^T A_{\omega_0}\,dt\right|^2 M/2 = MA_{\omega_0}{}^2\lambda^2/2c^2 \quad (6)$$

The derivation of eq 6 involves several assumptions. First, we assume that there is a harmonic with a frequency equal to a resonance one; otherwise eq 6 would give no energy transfer. For a realistic system with dissipation, however, the resonance peak has a finite width, and, since the frequency of the primary harmonic is typically much smaller than the resonance frequency, one or even several neighboring harmonics may be able to couple with the surface species. Moreover, the acoustic pulse generated by laser irradiation in LIAD experiments has a continuous broadband spectrum, and the representation of this spectrum by the discrete harmonics is just a numerical approximation of eq 1, the general equation provided by the Fourier transform of the wave profile. While the assumption of a single resonance frequency may result in underestimation of the energy transferred by the wave to the adsorbate, the neglect of the energy flow in the opposite direction, from the vibrationally excited adsorbate to the substrate, has an opposite effect on the predicted energy transfer. Despite the rather strong assumptions used in the derivation of eq 6 and the ambiguity with defining A_{ω_0}, the application of this equation for the description of the MD simulation results presented in sections 3.2 and 4suggests that it provides not only the general scaling law but also a reliable semiquantitative estimate of the conditions for the desorption of atomic clusters and exfoliation of thin graphene multilayers.

3.2. MD Simulation of Acoustic Desorption of Atomic Clusters. The MD simulations of acoustic desorption of atomic clusters are performed for bulk longitudinal waves with an initial wavelength of $\lambda = 935\sigma$ and different strain amplitudes. The conditions for acoustic desorption are expected to be optimal when the nonlinear sharpening of the wave profile leads to the formation of a well-developed shock front, so that A_{ω_0} in eq 6 is maximized. Therefore, in most of the simulations, the time for the introduction of the surface and adsorbates into the simulation system is chosen to ensure that the surface is exposed to the incoming shock front. Since the surface is introduced at the position of zero strain, it takes about half of the wave period ($\sim 50\tau$) for the wave front to reach the surface, and the optimal time is $\sim 50\tau$ prior to the shock formation.

Note that extending the time of the wave propagation beyond what is needed for the shock wave formation does not result in a further increase in the desorption efficiency. On the contrary, the formation of the shock front signifies the rapid increase in the rate of the energy dissipation,[54,55] which balances the rate of nonlinear frequency upconversion and suppresses the further increase of the frequencies of higher-order harmonics (front sharpening). The onset of the rapid energy dissipation is actually used in the present study to evaluate the distance of the shock front formation for waves with different initial strain amplitudes. The total energy of a wave is calculated by summing the contributions of individual harmonics defined as $C_{11}(A^e_\omega)^2/2$, where C_{11} is an elastic constant and A^e_ω is the amplitude in the strain spectrum at frequency ω computed with the discrete Fourier transform applied to the evolving wave profiles. For waves with initial strain amplitudes of 0.0628, 0.0314, and 0.0157, the simulations reveal the onset of rapid energy dissipation at 0.63λ, 1.34λ, and 2.60λ propagation distances, which correspond to 64τ, 136τ, and 263τ, respectively. The shock front formation distance for an initially sinusoidal wave is commonly described as $L_{sh} = 1/\beta e_0 k$,[40,56] where β is the effective nonlinearity parameter of the material. Based on the shock formation distances evaluated in the simulation for different e_0, $\beta \approx 4$, which is in the range of 4−8 measured for various crystalline and amorphous materials.[57] The nonlinear evolution of the bulk waves in the model LJ system considered in the present work, therefore, can be expected to be similar to that occurring in real materials.

Once the waves are generated and the surfaces with adsorbed clusters are introduced as described above, the

https://doi.org/10.1021/acs.jpcc.1c07311
J. Phys. Chem. C 2021, 125, 23313−23326

ability of the waves to desorb the clusters in a single wave period is investigated. For each set of the wave parameters (wave amplitude and the time of the surface exposure to the wave), a series of simulations is performed for a range of cluster binding energies E_b. The number of clusters desorbed from the surface is determined in each simulation, and the desorption probability, defined as the probablility of a cluster to desorb during the simulation, is calculated for each binding energy. The dependence of the desorption probability on the binding energy is then fitted to a sigmoid function, and the threshold binding energy, E_b^{th}, is identified. The latter is defined as a binding energy for which a 0.5 desorption probability is observed.

We first consider strong waves with an initial strain amplitude of 0.0628. The atoms in the clusters deposited on the surface have a mass of $m_c = 1.74m$, i.e., the total mass of each cluster is $17.4m$. In the simulations illustrated by Figure 2c, we do not allow any time for the wave to evolve prior to the introduction of the surfaces and adsorbates. The surface introduction procedure, however, ensures that the part of the wave that evolves into the shock front is located about half of the wave period away from the surface and has $\sim 50\tau$ to propagate before reaching the surface. This evolution leads to a substantial distortion/sharpening of the initially sinusoidal wave profile, as can be seen from Figure 2a. Even though the shock front is not yet formed at the time of the wave interaction with the surface, and the corresponding spectrum has only a relatively small population of high-frequency harmonics (Figure 2b), the desorption of clusters caused by the reflection of the wave from the surface is clearly distinguishable from purely thermal desorption at the nominal substrate temperature of $0.1\varepsilon/k_B$. The plot of the desorption probability versus cluster binding energy in Figure 2c yields the threshold value of $E_b^{th} = 0.76\varepsilon$, which is substantially higher than the binding energies for which the thermally activated desorption could be observed at the substrate temperature.

The probability of thermal desorption, also plotted in Figure 2c, is calculated based on the Arrhenius equation for the desorption rate r_d:

$$r_d = \nu_0 \exp(-E_b/k_B T_s) \tag{7}$$

where k_B, T_s, and $\nu_0 = \omega_0/2\pi$ are the Boltzmann constant, surface temperature, and the characteristic frequency of cluster vibrations. Since the mass of the clusters stays constant as the binding energy is varied in the simulations, the characteristic frequency of cluster vibrations is estimated as $\nu_0 = \nu^* \sqrt{E_b/E_b^0}$, where ν^* of $0.322\tau^{-1}$ is evaluated based on the position of the peak in the natural cluster vibrational frequency spectrum for the vertical oscillations of a cluster with an E_b^0 of 21.2ε (used in the previous study of the acoustic activation of surface diffusion[45]). The probability of thermal desorption in a sequence of desorption attempts during the time of the simulation t_s can be approximated with Poisson distribution using the Poisson limit theorem, so that

$$p_d^T = 1 - \exp(-r_d t_s) \tag{8}$$

The time t_s used in the evaluation of the thermal desorption is taken to be 60τ, which is close to the time of the interaction of the acoustic pulse with the surface. The description of thermal desorption by eqs 7 and 8 is consistent with the Polanyi–Wigner equation[58] for the first-order desorption of individual clusters without redeposition. Note that, due to the dependence of ν_0 on E_b, p_d^T predicted by eqs 7 and 8 and plotted in Figure 2c does not approach unity as E_b decreases to 0 but peaks at $E_b \approx 0.05\varepsilon$, when $1/\nu_0 \approx t_s$.

The effect of the acoustic desorption is considerably stronger if the wave is allowed to propagate for a time sufficiently long for the shock wave formation. For a wave with the same initial strain amplitude of 0.0628, the shock front is fully formed by 150τ, as can be seen from the wave profile plotted in Figure 2d and the corresponding frequency spectrum shown in Figure 2e. The simulation where the surface is introduced at 100τ and the shock front reflects from the surface at $\sim 150\tau$ predicts the 50% desorption probability for clusters with binding energies as high as 6.1ε. To reproduce the same desorption probability on the simulation time scale by thermal desorption mechanism, the temperature of the substrate should be $2.25\varepsilon/k_B$, which is more than 20 times higher than the actual substrate temperature. In the model used in the simulations, the resonance frequency of a cluster is proportional to the square root of the binding energy. Therefore, as indicated by the shift of the blue arrow in Figure 2e to higher frequencies with respect to the blue arrow in Figure 2b, the desorption of clusters with higher binding energies requires an increase in the amplitudes of higher frequency harmonics matching the vibrational modes of the surface species and enabling an effective energy transfer, as described by eq 6.

The amounts of energy transferred to a cluster calculated with eq 6 using the values of A_{ω_0} marked by blue arrows in Figure 2, parts b and e, are 4.4ε and 25.8ε for the wave profiles shown in Figure 2, parts a and d, respectively. These estimates of the transferred energy are substantially higher than the values of E_b^{th} predicted in the MD simulations, suggesting that the energy dissipation from the oscillator to the substrate and nonlinear effects ignored in the derivation of the equation may have a substantial effect on the energy exchange between the substrate and surface species. Despite the discrepancy, the qualitative behavior predicted by eq 6 and the frequency spectra calculations is confirmed in the MD simulations: the sharpening of the wave profile and the shock front formation lead to the desorption of clusters with higher binding energies.

One notable characteristic of the dependence of the desorption probability on the binding energy shown in Figure 2f is a relatively gradual decrease of the desorption probability with the increase of the binding energy. The lack of a sharp threshold-like behavior, expected for the acoustic desorption, may be partially attributed to the contribution of acoustically induced thermal effects. Specifically, in the simulation of the wave with the initial strain amplitude of 0.0628, the adiabatic compression and expansion of the LJ substrate by the wave[37] is found to result in ~20% temperature variation. Moreover, the onset of wave dissipation after the shock front formation leads to an additional temperature increase near the shock front, so that the maximum value of the temperature reaches $0.14\varepsilon/k_B$–$0.15\varepsilon/k_B$, and even $0.16\varepsilon/k_B$ at the time of the shock wave reflection from the surface. These temperatures are still much lower than the effective substrate temperature of $2.25\varepsilon/k_B$ that could yield the desorption probability observed in the simulation through the thermal desorption mechanism, thus suggesting that the thermal contribution only plays a supplementary role in the desorption process. Nevertheless, the contribution of the shock wave heating, along with the heat conduction through the substrate discussed in the Introduc-

https://doi.org/10.1021/acs.jpcc.1c07311
J. Phys. Chem. C 2021, 125, 23313–23326

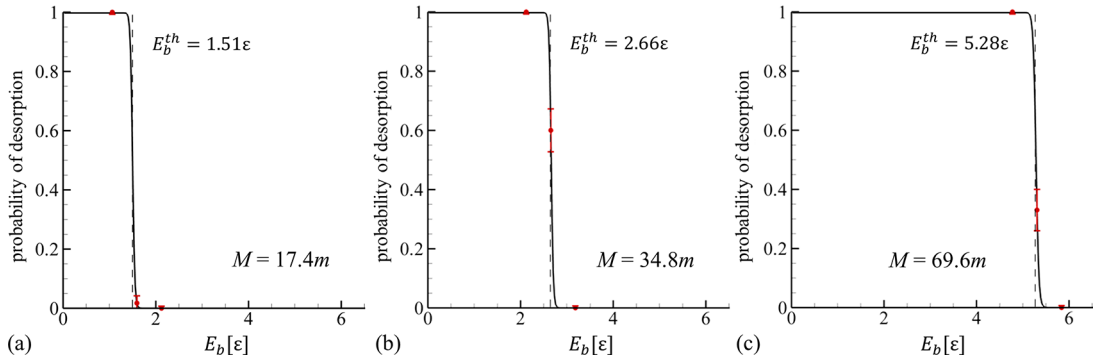

Figure 3. Dependence of the probability of cluster desorption on the binding energy of clusters with masses of 17.4m (a), 34.8m (b), and 69.6m (c). The initial wave strain amplitude is 0.0314, and the wave propagates for 190τ before it reaches the free surface with deposited atomic clusters.

tion, to the extended desorption times observed in a number of experimental studies[14,23] cannot be excluded.

In order to further suppress the acoustically induced thermal effects, we have performed an additional series of simulations for waves with initial strain amplitudes of 0.0314. The twice weaker wave results in a 2-fold decrease of acoustically induced thermal effects produced by the adiabatic compression. Additionally, there is a large reduction of heating related to the wave dissipation at the shock front. Lower wave amplitude inhibits the generation of high-frequency harmonics, which play a major role in the dissipation. In particular, our simulations reveal a nearly cubic dependence of the energy loss rate on the initial wave amplitude for waves with e_0 ranging from 0.015 to 0.06. The combination of these two effects leads to the reduction of the maximum temperature observed in the simulation down to $\sim 0.11\varepsilon/k_B - 0.115\varepsilon/k_B$. As illustrated in Figure 3a, the suppression of the thermally induced effects leads to a very sharp dependence of the desorption probability on the binding energy, which is a clear sign of the acoustic nature of the desorption.

The sharp threshold for the onset of acoustic desorption also suggests an attractive opportunity for the selective desorption of species with specific binding energies. To further support the proposed mechanism of the acoustically activated desorption based on the resonant coupling of the adsorbates with the high-frequency harmonics of the wave, we performed a series of simulations for different masses of atoms in the clusters, $m_c = 1.74m$, $3.48m$, and $6.96m$. According to eq 6, the energy transferred to a cluster and, therefore, the maximum binding energy of the desorbed clusters should be proportional to the mass of the cluster, $M = 10m_c$. The results of the simulations shown in Figure 3 match this theoretical prediction very well. Indeed, the increase of M from 17.4m to 34.8m and to 69.6m leads to a nearly linear increase of the threshold binding energy, E_b^{th}, from 1.51ε to 2.66ε and to 5.28ε. Since the probability of desorption through the purely thermal mechanism should be nearly independent of the cluster mass and controlled by the ratio of the binding energy to the substrate temperature, the results of this series of simulations unambiguously confirm the proposed acoustic desorption mechanism.

It is instructive to draw a connection between the model of acoustic desorption discussed above and the criterion for the desorption through the shake-off mechanism[14] briefly discussed in the Introduction, $v > v_{min} = \sqrt{2E_b/M}$. Using the connection between the strain and velocity amplitudes given by eq 5, the shake-off criterion can be reformulated in terms of the minimum initial strain amplitude of the wave leading to the desorption:

$$e_0 > e_{min} = \sqrt{2E_b/Mc^2} \tag{9}$$

The shake-off model, however, does not account for the need for the resonant coupling between the acoustic excitation and the adsorbate, and it simply gives an estimate by considering an instantaneous change of the surface velocity from 0 to v. A more realistic treatment accounting for the resonant coupling is given by eq 6, which can be reformulated into a form similar to that of eq 9 by making an assumption that, after the shock front is formed, the amplitudes of the high-frequency harmonics of acceleration are proportional to the initial wave amplitude and are independent of frequency. This assumption does not have a solid physical grounding, as the amplitudes of the harmonics of acceleration are defined by the dynamic balance between the frequency upconversion pumping the energy to the higher frequency harmonics and the rapid dissipation of the high-frequency harmonics into the thermal phonons. Nevertheless, the independence on the frequency may be linked to the ultimate sawtooth shape of the shock waves. This shape gives $\sim 1/\omega$ asymptotic dependence of the Fourier transform components of strain and, therefore, constant amplitudes in the spectrum of acceleration (due to the multiplication by ω). At a semiquantitative level, this assumption is empirically supported by the frequency spectra shown in Figure 2e, where the acceleration amplitudes can be seen to exhibit a rather weak frequency dependence. If we introduce a dimensionless coefficient α characterizing the assumed proportionality between A_{ω_0} and e_0, so that $A_{\omega_0} = e_0c^2/\alpha\lambda$, the desorption condition of $E > E_b$ based on eq 6 can be formulated in a form similar to that of eq 9:

$$e_0 > e_{min} = \alpha\sqrt{2E_b/Mc^2} \tag{10}$$

The coefficient α, representing the efficiency of the high-frequency harmonics generation and implicitly accounting for the requirement of the resonance condition, can be evaluated for each series of MD simulations performed for a given set of M and e_0. The values of E_b^{th} evaluated in the simulations, along with the corresponding values of α calculated with eq 10 using $E_b = E_b^{th}$, $e_{min} = e_0$, and $c = 9.23\ \sigma/\tau$, are listed in Table 1. The fact that the computed values of α remain within a relatively narrow range of 0.69−0.74 for the 2-fold variation of the wave amplitude and the 4-fold variation of the mass of the adsorbates suggests that the assumption of the linear relationship between the amplitudes of high-frequency

https://doi.org/10.1021/acs.jpcc.1c07311
J. Phys. Chem. C 2021, 125, 23313−23326

Table 1. Threshold Binding Energy, E_b^{th}, Defined as 0.5 Desorption Probability, and Coefficient α, Representing the Efficiency of the High-Frequency Harmonic Generation, Determined in Simulations Performed for Atomic Clusters of Mass M and Acoustic Waves with a Strain Amplitude of e_0

e_0	M	E_b^{th}	α
0.0628	17.4	6.1	0.692
0.0314	17.4	1.51	0.695
0.0314	34.8	2.66	0.741
0.0314	69.6	5.28	0.744

harmonics of acceleration and the initial wave amplitude (after the shock front is fully formed) works reasonably well.

An observation that the value of α is less than unity appears to suggest, from first sight, that the consideration of nonlinear wave sharpening and resonant coupling to the surface species gives a higher desorption efficiency than the shake-off approximation, which is supposed to give the lower bound estimate of the wave amplitude required for the desorption. The consideration of the simulated wave profiles (e.g., Figure 2d) suggests, however, that the velocity of the surface is not changing from 0 to v, as assumed in the shake-off model, but is slowly decreasing from 0 to $-v$ and then suddenly changing to v at the shock front. The magnitude of the instantaneous change of the velocity in the shake-off approximation for such wave profiles, therefore, should be $2v$, and the shake-off estimate of the minimum strain amplitude becomes $e_{min} = 0.5\sqrt{2E_b/Mc^2}$. The values of α predicted in the simulations, 0.69−0.74, are indeed larger than the lower bound estimate provided by the shake-off approximation. For a typical pressure pulse generated by short-pulse laser irradiation (compressive component followed by a weaker tensile one),[26−30] the original shake-off estimation given by eq 9 should be related to eq 10 with a value of α increased by a factor of 2.

Mapping the computational predictions to the conditions of LIAD experiments can be done by assuming typical values of the speed of sound in metals, 5000 m/s,[59] binding energies of analyte molecules, 0.05−0.5 eV, and their masses, 100−1000 Da.[14] Using these values in eq 10, the strain amplitude of the wave required for the desorption can be estimated to be of the order of 10^{-2}−10^{-1}. This level of strain can be readily produced by ultrashort pulse laser irradiation of metal targets, which leads to rapid localized heating occurring under conditions of stress confinement.[27,30] With the nanosecond laser pulses, sufficiently strong pressure pulses with strains of the order of ∼0.01[60] can be generated in the regime of laser ablation, when a large compressive pressure can be exerted on the target by an explosive phase decomposition[27,61−63] of a surface region of the irradiated substrate or an absorbing layer deposited to the substrate.[60,64] The pressure can be further increased when the ablation or thermoelastic expansion is spatially confined by a transparent overlayer.[18,19,28−30]

In cases when surface species form clusters, small islands, of several-monolayer-thick layers on the surface, the effective ratio of E_b/M in eq 10 may decrease, leading to the reduction of the wave strain amplitude required for the acoustic desorption. When the deposited layer gets thicker than several monolayers, however, the consideration of the resonant coupling of the high-frequency wave harmonics to the adsorbate is no longer applicable, and the molecular ejection needs to be considered in the continuum framework, in a manner analogous to back surface spallation caused by the wave reflection.[26] The transition from the resonant coupling to the spallation regime is illustrated in section 4 for the exfoliation of multilayer graphene.

4. ACOUSTIC EXFOLIATION OF GRAPHENE MULTILAYERS

The mechanisms of acoustically driven ejection/exfoliation of continuous overlayers are investigated for a realistic system of multilayer graphene on a Cu substrate with (111) surface orientation. The Cu substrates have been demonstrated to be effective in chemical vapor deposition (CVD) growth of both large-area graphene[65−67] and small graphene islands[68] with a controlled number of layers. One of the remaining challenges in the utilization of graphene layers as elements of electronic and optoelectronic devices is the transfer of the graphene from a substrate to an acceptor. The common methods of chemical etching of Cu substrates[65,69] or electrochemical delamination of the graphene layers[70] are relatively slow and add significantly to the overall cost of the graphene device integration. The acoustic exfoliation may provide an attractive alternative approach to the detachment and transfer of the graphene multilayers from the catalytic growth substrate to the destination substrate. The noncontact chemical-free nature of the method may open up opportunities for the integration of acoustically induced transfer of graphene with other digital printing techniques[71−73] for fabrication of flexible electronics of functional nanocomposite films and coatings.

The direct application of eq 10 to the estimation of the conditions for the acoustically driven separation of single-layer graphene from a Cu(111) surface, performed with E_b = 117 meV/atom (see section 2.3), M = 12.0 Da, c = 4760 m/s,[59] and α = 0.7 (the value estimated based on the analysis of acoustic desorption of atomic clusters described in section 3.2) yields strain amplitude $e_{min} \sim 0.20$. This estimation suggests that the relatively strong interaction of a single-layer graphene with a Cu(111) surface is likely to prevent the detachment of a monolayer through the mechanism that assumes the direct coupling of high-frequency harmonics of nonlinear bulk acoustic waves to the vibrational modes of the graphene monolayer. The interaction between graphene sheets is substantially weaker than the interaction between graphene and the Cu substrate. In particular, in the model describing interatomic interactions with AIREBO potential,[48] the value of E_b is 41.0 meV/atom for the separation of two graphene layers from each other, which reduces e_{min} to ∼0.12 for the separation of single-layer graphene from a bilayer. Note that in this estimation we neglect the possibility of distortions of the graphene sheet and assume a simultaneous removal of all atoms in a flat layer, which may lead to an overestimation of the wave strength required for the layer separation. Moreover, for the simultaneous ejection of multiple layers of graphene, the parameter M should be increased proportionally to the number of layers, leading to a further decrease of the required strain.

To test the validity of these estimations, we have performed a series of MD simulations of single-, double-, and four-layer graphene, as well as a thicker 25-layer graphite overlayer, deposited on a Cu substrate. The nonlinear waves with strain amplitudes of 0.04 and 0.06 are generated by using the computational "synchrotron" approach described in section 2.1. At these strain amplitudes, the waves are found to cause no

https://doi.org/10.1021/acs.jpcc.1c07311
J. Phys. Chem. C 2021, 125, 23313−23326

damage to the Cu substrate during their propagation in the substrate and reflection from the surface. Before the surface with graphene is introduced, the waves were allowed to propagate for 70 and 40 ps for waves with 0.04 and 0.06 strain amplitudes, respectively. These times of free wave propagation are chosen so that the nonlinear sharpening of the wave profiles produces fully developed shock fronts by the time the waves reach the surfaces covered by the overlayers.

The response of the overlayers to the exposure of the surface to the shock waves is illustrated by snapshots from the MD simulations shown in Figure 4. Only the top parts of the

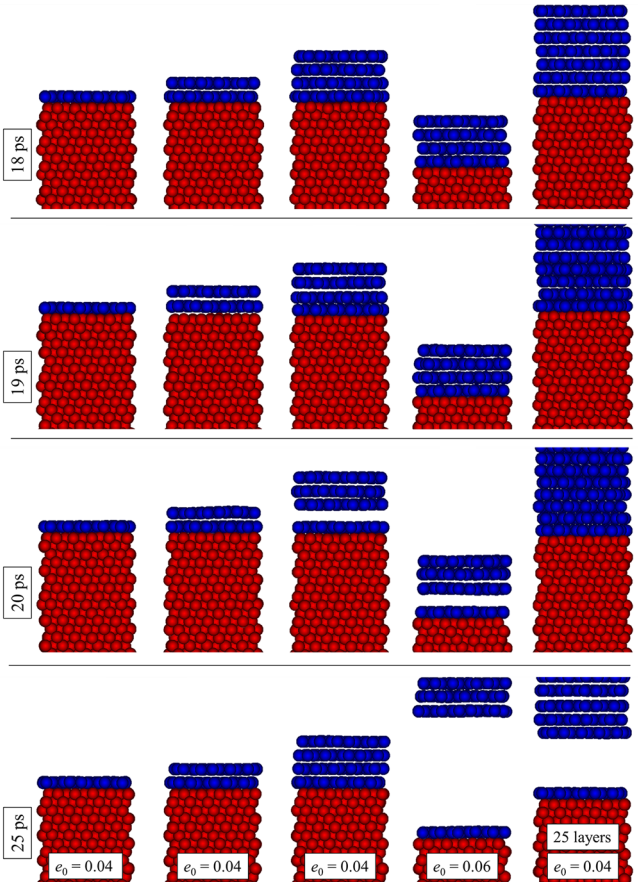

Figure 4. Snapshots from MD simulations of response of Cu substrate covered by single-layer and multilayer graphenes to a nonlinear acoustic pulse coming from the bulk of the Cu substrate and reflecting from the surface. The snapshots are shown for systems with single-, double-, and four-layer graphenes, as well as a 25-layer graphite overlayer. The time labeled on the figure is counted from the moments when the surfaces and the overlayers are introduced in the simulations. The wave strain amplitudes, e_0, are marked on the figure. Only the top parts of the Cu substrate and the lower part of the 25-layer graphite overlayer are shown in the snapshots. The Cu and C atoms are colored red and blue, respectively.

systems with graphene single layer or multilayers and the Cu−graphite interfacial region of the system with 25-layer graphite overlayer are depicted in Figure 4. The time labeled on the figure is counted from the moments when the surfaces and the overlayers are introduced, i.e., 70 and 40 ps after the start of the simulations with waves of 0.04 and 0.06 strain amplitudes, respectively. The wave with e_0 = 0.04 is not observed to lead to the ejection of the graphene layers. For the two-layer graphene system, the shock wave reflection from the surface at ∼19 ps results in a slight change of the distance between the substrate and graphene as well as between the two graphene layers. For the four-layer graphene, the top three layers are transiently detached from the first layer by 20 ps, but the upward motion of the substrate produced by the approaching compressive component of the wave leads to the reattachment by 25 ps.

The increase of the wave strain amplitude to 0.06 leads to the detachment and ejection of the top three layers from the four-layer graphene system. The detachment of only three layers is defined by the weaker graphene−graphene interlayer interaction (41.0 meV/atom) as compared to the graphene interaction with the Cu substrate (117 meV/atom). The strain amplitude required for the separation of the three layers for four-layer graphene on a Cu substrate can be estimated with eq 10, using parameters E_b = 41 meV/atom, M = 36 Da, c = 4760 m/s, and α = 0.7. This estimation gives e_{min} = 0.07, which is close to the strain of 0.06 observed to cause the ejection of the three layers in the MD simulation. Given that the parameter α used in the estimation of e_{min} is computed for a model LJ system and the desorption of atomic clusters, the observed agreement is remarkable and indicates that the physical picture captured by eq 10 is applicable to a wide range of systems and surface species.

The thickness of 25-layer graphite is much larger than the thickness of the shock front, which is several nanometers in the simulations. Therefore, the interaction of bulk waves with a 25-layer graphite overlayer cannot be described by eq 10, in terms of the resonant coupling of the high-frequency harmonics generated at the shock front to the surface species. Instead, the ejection of the thick overlayer can be treated at the continuum level, by considering the reflection, transmission, and interaction of stress waves in the surface region of the system.

The temporal and spatial evolution of the normal stress, σ_{zz}, in the Cu substrate and graphite overlayer is depicted in Figure 5 for the wave with e_0 = 0.04. The propagation of the shock

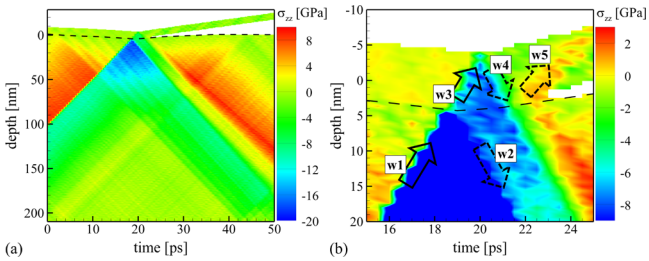

Figure 5. Temporal and spatial evolution of normal stress, σ_{zz}, in the Cu substrate and graphite overlayer predicted in the simulation illustrated by snapshots shown in the right column of Figure 4. A view zoomed on the surface region and the time of the shock wave interaction with the overlayer is shown in (b). The black dashed line shows the location of the Cu surface. Solid and dashed arrows in (b) illustrate the direction of propagation of compression and rarefaction waves produced by transmission and reflection of the incoming shock wave denoted as w1.

front causing the sudden compression of the material expanded by the preceding tensile component of the wave is denoted as w1 in Figure 5b. The shock front reaches the Cu−graphite interface at about 19 ps and partially reflects from the interface as a rarefaction wave w2. Meanwhile, the incident wave (w1) partially propagates into the graphite overlayer (w3) and reflects from the top free surface of the graphite overlayer as a rarefaction wave w4. The wave w4 partially reflects from the

https://doi.org/10.1021/acs.jpcc.1c07311
J. Phys. Chem. C 2021, 125, 23313−23326

graphite−Cu interface as a rarefaction wave w5, leading to the concentration of the tensile stresses in the interfacial region strong enough for the separation/spallation of the graphite overlayer from the substrate.

To quantify the reflection and transmission of the waves in the surface region of the Cu−graphite system, we need to consider the specific acoustic impedance of the two materials. The specific acoustic impedance in Cu along the [111] wave propagation direction can be calculated as[54]

$$z_{Cu} = \sqrt{(C_{11} + 2C_{12} + 4C_{44})\rho/3}$$

At 300 K, the EAM potential[47] used in this study gives C_{11} = 163.52 GPa, C_{12} = 120.06 GPa, C_{44} = 71.44 GPa, and ρ = 8811 kg/m^3, which yields $z_{Cu} = 4.50 \times 10^7$ Pa·s/m. The specific acoustic impedance of graphite is computed as $z_C = \sqrt{C_{33}\rho} = 0.94 \times 10^7$ Pa·s/m for C_{33} = 38.7 GPa and ρ = 2261 kg/m^3.[74] For a wave transmission from material 1 to material 2, the reflection and transmission coefficients for stress amplitudes are given by the following equations (here we consider the amplitude coefficients, while the intensity coefficients are computed as squares of the amplitude coefficients):[75,76]

$$R = (z_2 - z_1)/(z_1 + z_2) \quad (11)$$

$$T = 2z_2/(z_1 + z_2) \quad (12)$$

For a wave crossing the interface from Cu to graphite, $z_1 = z_{Cu}$ and $z_2 = z_C$, while for the wave moving in the opposite direction $z_1 = z_C$ and $z_2 = z_{Cu}$. Therefore, $R_{Cu\to C} = -0.66$, $T_{Cu\to C} = 0.34$, $R_{C\to Cu} = 0.66$, and $T_{C\to Cu} = 1.66$. The stress amplitude of the incident compressive wave (w1) is $\sigma_{zz} = -(C_{11} + 2C_{12} + 4C_{44})e_0/3 = -9.2$ GPa, and a stress amplitude of the wave transmitted into graphite (w3) is thus −3.2 GPa. It should be noted that the actual values of stress observed in Figure 5 are defined by the overlap of the incident and reflected waves, so that, for example, the maximum stress generated near the surface of the Cu substrate reaches about −20 GPa at ∼19 ps. The wave reflected from the free surface (w4) has a stress amplitude of 3.2 GPa, the same as that of w3, but with the opposite sign ($R = -1$, $T = 0$ at the free surface). This wave then reflects from the graphite−Cu interface producing a tensile wave (w5) with a stress amplitude of 2.1 GPa. The interaction between the incoming (w4) and reflected (w5) rarefaction waves generates the tensile (positive) stresses at the graphite−Cu interface that are sufficiently high to cause the separation and ejection of the graphite overlayer from the Cu substrate. The snapshots from the simulation shown in Figure 4 illustrate the ejection of the graphite overlayer that leaves behind only one graphene layer that is more strongly bonded to the Cu substrate as compared to the second graphene layer.

Overall, the computational results suggest an attractive opportunity of using the acoustic stimulus for a noncontact removal of overgrown multilayer parts of graphene films formed on catalytic substrates in CVD growth, while keeping the single-layer graphene regions intact. Moreover, the predicted sensitivity of the wave amplitude threshold for the graphene exfoliation to the thickness of the multilayers may enable real-time control over the thickness of the growing films by changing the amplitude of the acoustic waves. The acoustic exfoliation explored in the present study for the Cu(111)−graphene system can also be applied to graphene grown on other substrates,[77−79] as well as to other 2D materials.[80−82] For systems with weaker overlayer−substrate interactions, the requirement on the strength of the acoustic waves can be relaxed, thus facilitating the integration of the acoustic exfoliation into the existing synthesis processes.

At a qualitative level, the computational results obtained for the acoustic exfoliation of graphene multilayers can provide some initial insights into the mechanisms responsible for the ejection and volatilization of analyte molecules in LIAD mass spectrometry experiments performed for continuous molecular overlayers.[12,13,15−25] For the overlayers with a thickness comparable to or thinner than that of the shock front of the acoustic pulses, the molecular ejection can be caused by the direct resonant coupling of the overlayer to the high-frequency harmonics associated with the formation of the shock front. For thicker overlayers, the mechanical spallation driven by the shock wave transmitted into the overlayer and reflected from the free surface of the sample is the mechanism that is likely to be responsible for the collective ejection of the overlayer. The subsequent processes leading to the fragmentation of the ejected overlayer and volatilization of analytes are likely to be system-specific and require further analysis accounting for the molecular structure of the overlayer.

5. SUMMARY

The mechanisms of acoustically activated desorption of atomic clusters and exfoliation of graphene multilayers are investigated in MD simulations that account for the nonlinear sharpening of the acoustic waves during their propagation through the substrates. The results for the atomic clusters clearly demonstrate a nonthermal nature of desorption from surfaces exposed to strong nonlinear acoustic waves. The desorption probability is found to be sensitive to the extent of nonlinear sharpening of the wave profile, which is defined by the nonlinearity of the elastic properties of the substrate material, the wave amplitude, and the distance traveled by the wave through the substrate. For acoustic pulses with well-developed shock fronts, sharp threshold-like dependences of the desorption probability on the binding energy of the adsorbates are observed in the simulations, which highlight the nonthermal nature of the desorption process. Indeed, the effective substrate temperature that could yield the desorption probability observed in the simulation through the thermal desorption mechanism is estimated to be more than 20 times higher than the actual substrate temperature. A nearly linear dependence of the threshold binding energy for the acoustic desorption on the mass of the adsorbates, observed in the simulations, can also be contrasted to the thermal desorption that should be independent of the cluster mass and controlled by the ratio of the binding energy to the substrate temperature.

The results of MD simulations are described by a simple semiempirical (i.e., parametrized based on the results of computer experiments) model based on the consideration of the resonant coupling of high-frequency harmonics of the nonlinear acoustic waves with the vibrational modes of the adsorbates. The analysis of the resonant energy transfer to the adsorbates yields a general scaling law describing the dependence of the minimum strain amplitude of the wave required for the desorption on the binding energy and mass of the adsorbates. The fitting of the analytical equation to the results of MD simulations performed for adsorbates with different masses and binding energies demonstrates that the equation can provide a reliable semiquantitative estimate of the conditions for the desorption of atomic clusters.

https://doi.org/10.1021/acs.jpcc.1c07311
J. Phys. Chem. C 2021, 125, 23313−23326

The extension of the investigation from the acoustic desorption of isolated adsorbates to the ejection/exfoliation of continuous overlayers of adsorbates is done by performing MD simulations of Cu(111) substrate covered with single-layer graphene, multilayer graphene, and a thicker graphite overlayer. In addition to the exploration of an intriguing possibility of using the acoustic energy for exfoliation and transfer of graphene from metal surfaces, this system provides some general insights into the mechanisms that may be involved in the molecular ejection from continuous layers of analyte samples, commonly used in LIAD. The results of the simulations demonstrate the ability of strong nonlinear acoustic pulses to cause the separation and ejection of three-layer graphene while keeping a single graphene layer on the substrate. The minimum strain amplitude of the wave required for the exfoliation of the multilayer graphene is found to be in good agreement with estimates provided by the semiempirical equation parametrized based on the MD results for desorption of atomic clusters. This agreement suggests that the physical picture captured by the analytical model and the corresponding semiempirical expression are applicable to a wide range of systems and surface species.

As the thickness of the graphene/graphite multilayer increases and exceeds the thickness of the shock front of the wave (several nanometers, or about 10 graphene layers), the description of the acoustically driven ejection of the multilayer in terms of the resonant coupling of the high-frequency wave harmonics to the overlayer vibrations is no longer applicable. The ejection of the overlayer, in this case, can be described at the continuum level, in a manner analogous to the description of back surface spallation caused by the wave reflection. This approach is exemplified by the results of MD simulation of a Cu substrate covered by a 25-layer-thick graphite overlayer. The separation and ejection of all but a single graphene layer from the substrate are explained by considering the reflection, transmission, and interaction of stress waves in the surface region of the system.

The unifying aspect of both the energy transfer through the resonant coupling to the vibrational states of the adsorbates and the spallation-like ejection of a thin overlayer is the requirement for the nonlinear sharpening of the acoustic waves leading to the shock front formation. The laser-generated broadband acoustic pulse in LIAD, therefore, should be sufficiently strong to facilitate the nonlinear evolution into a shock wave, while the distance from the wave source to the surface should be long enough for the shock front formation, but not too long to minimize the active wave dissipation at the shock front.

The improved understanding of the mechanisms of acoustic desorption provided by the present study can have important implications for various fields ranging from cold desorption of heat-sensitive molecules for mass spectrometry analysis to the removal of products of chemical reactions and regeneration of the catalytic activity of metal surfaces. The existence of a sharp binding energy threshold for the acoustic desorption, predicted in the simulations, may enable selective desorption of surface species with specific binding energies. The demonstration of the feasibility of the acoustic exfoliation of multilayer graphene may facilitate the development of new experimental tools utilizing the acoustic energy for *in situ* control over the thickness of growing multilayer films or for acoustically induced detachment and transfer of 2D materials from a growth substrate to a precisely targeted destination in the device manufacturing.

AUTHOR INFORMATION

Corresponding Author

Leonid V. Zhigilei − *Department of Materials Science and Engineering, University of Virginia, Charlottesville, Virginia 22904-4745, United States;* orcid.org/0000-0002-1549-7086; Email: lz2n@virginia.edu

Author

Maxim V. Shugaev − *Department of Materials Science and Engineering, University of Virginia, Charlottesville, Virginia 22904-4745, United States*

Complete contact information is available at: https://pubs.acs.org/10.1021/acs.jpcc.1c07311

Notes

The authors declare no competing financial interest.

ACKNOWLEDGMENTS

Financial support for this work was provided by the National Science Foundation (NSF) through Grant No. CMMI-1562929. Computational support was provided by the NSF through the Extreme Science and Engineering Discovery Environment (Project No. TGDMR110090) and by Research Computing at the University of Virginia.

REFERENCES

(1) Denison, D. R. Phonic desorption. *J. Vac. Sci. Technol.* **1969**, *6*, 214−217.

(2) Krischer, C.; Lichtman, D. Observation of desorption from quartz induced by surface acoustic waves. *Phys. Lett. A* **1973**, *44*, 99−100.

(3) Basov, N. G.; Belenov, E. M.; Gubin, M. A.; Kurdoglyan, M. S.; Nikitin, V. V.; Oraevskiĭ, A. N.; Chichkov, B. N. New ways of obtaining cold atoms and molecules. *Sov. J. Quantum Electron.* **1987**, *17*, 919−922.

(4) Kelling, S.; Cerasari, S.; Rotermund, H. H.; Ertl, G.; King, D. A. A photoemission electron microscopy (PEEM) study of the effect of surface acoustic waves on catalytic CO oxidation over Pt{110}. *Chem. Phys. Lett.* **1998**, *293*, 325−330.

(5) Nishiyama, H.; Rattana, N.; Saito, N.; Sato, K.; Inoue, Y. Effects of Rayleigh surface acoustic wave upon adsorptive and surface properties of a thin NiO film. *J. Phys. Chem. B* **2000**, *104*, 10602−10607.

(6) von Boehn, B.; Foerster, M.; von Boehn, M.; Prat, J.; Macià, F.; Casals, B.; Khaliq, M. W.; Hernández-Mínguez, A.; Aballe, L.; Imbihl, R. On the promotion of catalytic reactions by surface acoustic waves. *Angew. Chem., Int. Ed.* **2020**, *59*, 20224−20229.

(7) Inoue, Y. Acoustic enhancement of surface reactions. *MRS Bull.* **2019**, *44*, 361−371.

(8) Lindner, B.; Seydel, U. Laser desorption mass spectrometry of nonvolatiles under shock wave conditions. *Anal. Chem.* **1985**, *57*, 895−899.

(9) Lindner, B. On the desorption of electrosprayed organic compounds from supporting metal foils by laser induced pressure waves. *Int. J. Mass Spectrom. Ion Processes* **1991**, *103*, 203−218.

(10) Golovlev, V. V.; Allman, S. L.; Garrett, W. R.; Chen, C. H. Laser-induced acoustic desorption of electrons and ions. *Appl. Phys. Lett.* **1997**, *71*, 852−854.

(11) Golovlev, V. V.; Allman, S. L.; Garrett, W. R.; Taranenko, N. I.; Chen, C. H. Laser-induced acoustic desorption. *Int. J. Mass Spectrom. Ion Processes* **1997**, *169−170*, 69−78.

(12) Pérez, J.; Ramírez-Arizmendi, L. E.; Petzold, C. J.; Guler, L. P.; Nelson, E. D.; Kenttämaa, H. I. Laser-induced acoustic desorption/

chemical ionization in Fourier-transform ion cyclotron resonance mass spectrometry. *Int. J. Mass Spectrom.* **2000**, *198*, 173−188.
(13) Shea, R. C.; Petzold, C. J.; Campbell, J. L.; Li, S.; Aaserud, D. J.; Kenttämaa, H. I. Characterization of laser-induced acoustic desorption coupled with a Fourier transform ion cyclotron resonance mass spectrometer. *Anal. Chem.* **2006**, *78*, 6133−6139.
(14) Zinovev, A. V.; Veryovkin, I. V.; Moore, J. F.; Pellin, M. J. Laser-driven acoustic desorption of organic molecules from back-irradiated solid foils. *Anal. Chem.* **2007**, *79*, 8232−8241.
(15) Shea, R. C.; Habicht, S. C.; Vaughn, W. E.; Kenttämaa, H. I. Design and characterization of a high-power laser-induced acoustic desorption probe coupled with a Fourier transform ion cyclotron resonance mass spectrometer. *Anal. Chem.* **2007**, *79*, 2688−2694.
(16) Zinovev, A. V.; Veryovkin, I. V.; Pellin, M. J. Laser-induced desorption of organic molecules from front- and back-irradiated metal foils. *AIP Conf. Proc.* **2009**, *1104*, 200−206.
(17) Cheng, S.-C.; Cheng, T.-L.; Chang, H.-C.; Shiea, J. Using laser-induced acoustic desorption/electrospray ionization mass spectrometry to characterize small organic and large biological compounds in the solid state and in solution under ambient conditions. *Anal. Chem.* **2009**, *81*, 868−874.
(18) Cheng, S.-C.; Huang, M.-Z.; Shiea, J. Thin-layer chromatography/laser-induced acoustic desorption/electrospray ionization mass spectrometry. *Anal. Chem.* **2009**, *81*, 9274−9281.
(19) Dow, A. M.; Wittrig, A. R.; Kenttämaa, H. I. Laser-induced acoustic desorption (LIAD) mass spectrometry. *Eur. J. Mass Spectrom.* **2012**, *18*, 77−92.
(20) Ehlert, S.; Walte, A.; Zimmermann, R. Ambient pressure laser desorption and laser-induced acoustic desorption ion mobility spectrometry detection of explosives. *Anal. Chem.* **2013**, *85*, 11047−11053.
(21) Sezer, U.; Wörner, L.; Horak, J.; Felix, L.; Tüxen, J.; Götz, C.; Vaziri, A.; Mayor, M.; Arndt, M. Laser-induced acoustic desorption of natural and functionalized biochromophores. *Anal. Chem.* **2015**, *87*, 5614−5619.
(22) Benham, K.; Hodyss, R.; Fernández, F. M.; Orlando, T. M. Laser-induced acoustic desorption atmospheric pressure photoionization via VUV-generating microplasmas. *J. Am. Soc. Mass Spectrom.* **2016**, *27*, 1805−1812.
(23) Huang, Z.; Ossenbrüggen, T.; Rubinsky, I.; Schust, M.; Horke, D. A.; Küpper, J. Development and characterization of a laser-induced acoustic desorption source. *Anal. Chem.* **2018**, *90*, 3920−3927.
(24) Benham, K.; Fernández, F. M.; Orlando, T. M. Sweep jet collection laser-induced acoustic desorption atmospheric pressure photoionization for lipid analysis applications. *J. Am. Soc. Mass Spectrom.* **2019**, *30* (4), 647−658.
(25) Ma, X.; Zhang, Y.; Lei, H.-R.; Kenttämaa, H. I. Laser-induced acoustic desorption. *MRS Bull.* **2019**, *44*, 372−381.
(26) Paltauf, G.; Dyer, P. E. Photomechanical processes and effects in ablation. *Chem. Rev.* **2003**, *103*, 487−518.
(27) Shugaev, M. V.; He, M.; Levy, Y.; Mazzi, A.; Miotello, A.; Bulgakova, N. M.; Zhigilei, L. V. Laser-induced thermal processes: Heat transfer, generation of stresses, melting and solidification, vaporization and phase explosion. In *Handbook of Laser Micro- and Nano-Engineering*; Sugioka, K., Ed.; Springer: Cham, Switzerland, 2020.
(28) Anderholm, N. C. Laser-generated stress waves. *Appl. Phys. Lett.* **1970**, *16*, 113−115.
(29) Fabbro, R.; Fournier, J.; Ballard, P.; Devaux, D.; Virmont, J. Physical study of laser-produced plasma in confined geometry. *J. Appl. Phys.* **1990**, *68*, 775−784.
(30) Karim, E. T.; Shugaev, M.; Wu, C.; Lin, Z.; Hainsey, R. F.; Zhigilei, L. V. Atomistic simulation study of short pulse laser interactions with a metal target under conditions of spatial confinement by a transparent overlayer. *J. Appl. Phys.* **2014**, *115*, 183501.
(31) Peng, W.-P.; Yang, Y.-C.; Kang, M.-W.; Tzeng, Y.-K.; Nie, Z.; Chang, H.-C.; Chang, W.; Chen, C.-H. Laser-induced acoustic desorption mass spectrometry of single bioparticles. *Angew. Chem., Int. Ed.* **2006**, *45*, 1423−1426.
(32) Dzegilenko, F. N.; Uzer, T.; Herbst, E. Classical studies of shock wave-induced desorption for model adsorbates. *J. Chem. Phys.* **1996**, *105*, 10868−10873.
(33) Almeida, R.; Hood, E. S. Nonequilibrium dynamics in thermal desorption. *J. Phys. Chem.* **1992**, *96*, 3086−3092.
(34) Schroeder, M.; Wolf, D. E. Diffusion on strained surfaces. *Surf. Sci.* **1997**, *375*, 129−140.
(35) Mavrikakis, M.; Hammer, B.; Nørskov, J. K. Effect of strain on the reactivity of metal surfaces. *Phys. Rev. Lett.* **1998**, *81*, 2819−2822.
(36) Wu, M. W.; Metiu, H. The effect of strain on the adsorption of CO on Pd(100). *J. Chem. Phys.* **2000**, *113*, 1177−1183.
(37) Wu, C.; Zaitsev, V. Yu; Zhigilei, L. V. Acoustic enhancement of surface diffusion. *J. Phys. Chem. C* **2013**, *117*, 9252−9258.
(38) Kelling, S.; Mitrelias, T.; Matsumoto, Y.; Ostanin, V. P.; King, D. A. Acoustic wave enhancement of the catalytic oxidation of carbon monoxide over Pt {110}. *J. Chem. Phys.* **1997**, *107*, 5609−5612.
(39) Kelling, S.; King, D. A. Acoustic wave enhancement of catalytic reaction rates over platinum surfaces. *Platinum Metals Rev.* **1998**, *42*, 8−10.
(40) Rudenko, O. V.; Soluyan, S. I. *Theoretical Foundations of Nonlinear Acoustics*; Plenum Publishing Corp.: New York, 1977.
(41) Naugolnykh, L. K.; Ostrovsky, L. *Nonlinear Wave Processes in Acoustics*; Cambridge University Press: Cambridge, U.K., 1998.
(42) Shugaev, M. V.; Wu, C.; Zaitsev, V. Yu.; Zhigilei, L. V. Molecular dynamics modeling of nonlinear propagation of surface acoustic waves. *J. Appl. Phys.* **2020**, *128*, 045117.
(43) Stoddard, S. D.; Ford, J. Numerical experiments on the stochastic behavior of a Lennard-Jones gas system. *Phys. Rev. A: At., Mol., Opt. Phys.* **1973**, *8*, 1504−1512.
(44) Mastny, E. A.; de Pablo, J. J. Melting line of the Lennard-Jones system, infinite size, and full potential. *J. Chem. Phys.* **2007**, *127*, 104504.
(45) Shugaev, M. V.; Manzo, A. J.; Wu, C.; Zaitsev, V. Yu.; Helvajian, H.; Zhigilei, L. V. Strong enhancement of surface diffusion by nonlinear surface acoustic waves. *Phys. Rev. B: Condens. Matter Mater. Phys.* **2015**, *91*, 235450.
(46) Wu, C.; Zaitsev, V. Yu; Zhigilei, L. V. Mechanism of acoustically induced diffusional structuring of surface adatoms. *Appl. Phys. Lett.* **2013**, *103*, 221601.
(47) Williams, P. L.; Mishin, Y.; Hamilton, J. C. An embedded-atom potential for the Cu-Ag system. *Model. Simul. Mater. Sci. Eng.* **2006**, *14*, 817−833.
(48) Stuart, S. J.; Tutein, A. B.; Harrison, J. A. A reactive potential for hydrocarbons with intermolecular interactions. *J. Chem. Phys.* **2000**, *112*, 6472−6486.
(49) Sidorenkov, A. V.; Kolesnikov, S. V.; Saletsky, A. M. Molecular dynamics simulation of graphene on Cu (111) with different Lennard-Jones parameters. *Eur. Phys. J. B* **2016**, *89*, 220.
(50) Yoon, T.; Shin, W. C.; Kim, T. Y.; Mun, J. H.; Kim, T.-S.; Cho, B. J. Direct measurement of adhesion energy of monolayer graphene as-grown on copper and its application to renewable transfer process. *Nano Lett.* **2012**, *12*, 1448−1452.
(51) Xu, Z.; Buehler, M. J. Interface structure and mechanics between graphene and metal substrates: a first-principles study. *J. Phys.: Condens. Matter* **2010**, *22*, 485301.
(52) *LAMMPS Molecular Dynamics Simulator*. http://lammps.sandia.gov (accessed 2019-01-01).
(53) Landau, L. D.; Lifshitz, E. M. *Mechanics: Vol. 1 (Course of Theoretical Physics)*, 3rd ed.; Butterworth-Heinemann: 1976.
(54) Landau, L. D.; Lifshitz, E. M. *Theory of Elasticity*; Pergamon Press: 1989.
(55) Pitaevskii, L. P.; Lifshitz, E. M. *Course of Theoretical Physics: Physical Kinetics*; Elsevier Science: 2017.
(56) Blackstock, D. T. Nonlinear acoustics (theoretical). In *American Institute of Physics Handbook*, 3rd ed.; McGraw-Hill: New York, 1972; Chapter 3n.

https://doi.org/10.1021/acs.jpcc.1c07311
J. Phys. Chem. C 2021, 125, 23313−23326

(57) Zarembo, L. K.; Krasil'nikov, V. A. Nonlinear phenomena in the propagation of elastic waves in solids. *Sov. Phys. Usp.* **1971**, *13*, 778−797.
(58) King, D. A. Thermal desorption from metal surfaces: A review. *Surf. Sci.* **1975**, *47*, 384−402.
(59) *Handbook of Chemistry and Physics*, 64th ed.; Weast, R. C., Ed.; CRC Press: Boca Raton, FL, 1983.
(60) Kozhushko, V. V.; Lomonosov, A. M.; Hess, P. Intrinsic strength of silicon crystals in pure- and combined-mode fracture without precrack. *Phys. Rev. Lett.* **2007**, *98*, 195505.
(61) Martynyuk, M. M. Mechanism for metal damage by intense electromagnetic radiation. *Sov. Phys. Tech. Phys.* **1976**, *21*, 430−433.
(62) Kelly, R.; Miotello, A. Does normal boiling exist due to laser-pulse or ion bombardment? *J. Appl. Phys.* **2000**, *87*, 3177−3179.
(63) Bulgakova, N. M.; Bulgakov, A. V. Pulsed laser ablation of solids: transition from normal vaporization to phase explosion. *Appl. Phys. A: Mater. Sci. Process.* **2001**, *73*, 199−208.
(64) Kolomenskii, Al. A.; Lomonosov, A. M.; Kuschnereit, R.; Hess, P.; Gusev, V. E. Laser generation and detection of strongly nonlinear elastic surface pulses. *Phys. Rev. Lett.* **1997**, *79*, 1325−1328.
(65) Li, X.; Cai, W.; An, J.; Kim, S.; Nah, J.; Yang, D.; Piner, R.; Velamakanni, A.; Jung, I.; Tutuc, E.; Banerjee, S. K.; Colombo, L.; Ruoff, R. S. Large-area synthesis of high-quality and uniform graphene films on copper foils. *Science* **2009**, *324*, 1312−1314.
(66) Bhaviripudi, S.; Jia, X.; Dresselhaus, M. S.; Kong, J. Role of kinetic factors in chemical vapor deposition synthesis of uniform large area graphene using copper catalyst. *Nano Lett.* **2010**, *10*, 4128−4133.
(67) Seah, C.-M.; Chai, S.-P.; Mohamed, A. R. Mechanisms of graphene growth by chemical vapour deposition on transition metals. *Carbon* **2014**, *70*, 1−21.
(68) Wassei, J. K.; Mecklenburg, M.; Torres, J. A.; Fowler, J. D.; Regan, B. C.; Kaner, R. B.; Weiller, B. H. Chemical vapor deposition of graphene on copper from methane, ethane and propane: Evidence for bilayer selectivity. *Small* **2012**, *8*, 1415−1422.
(69) Chen, X.-D.; Liu, Z.-B.; Zheng, C.-Y.; Xing, F.; Yan, X.-Q.; Chen, Y.; Tian, J.-G. High-quality and efficient transfer of large-area graphene films onto different substrates. *Carbon* **2013**, *56*, 271−278.
(70) Wang, Y.; Zheng, Y.; Xu, X.; Dubuisson, E.; Bao, Q.; Lu, J.; Loh, K. P. Electrochemical delamination of CVD-grown graphene film: Toward the recyclable use of copper catalyst. *ACS Nano* **2011**, *5*, 9927−9933.
(71) Piqué, A.; Chrisey, D. B. *Direct-Write Technologies for Rapid Prototyping Applications*; Academic Press: San Diego, CA, USA, 2001.
(72) Hon, K. K. B.; Li, L.; Hutchings, I. M. Direct writing technology - Advances and developments. *CIRP Ann. - Manuf. Technol.* **2008**, *57*, 601−620.
(73) Serra, P.; Piqué, A. Laser-induced forward transfer: Fundamentals and applications. *Adv. Mater. Technol.* **2019**, *4*, 1800099.
(74) Bosak, A.; Krisch, M.; Mohr, M.; Maultzsch, J.; Thomsen, C. Elasticity of single-crystalline graphite: Inelastic x-ray scattering study. *Phys. Rev. B: Condens. Matter Mater. Phys.* **2007**, *75*, 153408.
(75) Landau, L. D.; Lifshitz, E. M. *Fluid Mechanics: Vol. 6 (Course of Theoretical Physics)*; Pergamon Press: 1982.
(76) Ohayon, R.; Soize, C. *Structural Acoustics and Vibration*; Academic Press: 1998.
(77) Mishra, N.; Boeckl, J.; Motta, N.; Iacopi, F. Graphene growth on silicon carbide: A review. *Phys. Status Solidi A* **2016**, *213*, 2277−2289.
(78) Pasternak, I.; Wesolowski, M.; Jozwik, I.; Lukosius, M.; Lupina, G.; Dabrowski, P.; Baranowski, J. M.; Strupinski, W. Graphene growth on Ge(100)/Si(100) substrates by CVD method. *Sci. Rep.* **2016**, *6*, 21773.
(79) Chen, Z.; Qi, Y.; Chen, X.; Zhang, Y.; Liu, Z. Direct CVD growth of graphene on traditional glass: Methods and mechanisms. *Adv. Mater.* **2019**, *31*, 1803639.
(80) Butler, S. Z.; Hollen, S. M.; Cao, L.; Cui, Y.; Gupta, J. A.; Gutiérrez, H. R.; Heinz, T. F.; Hong, S. S.; Huang, J.; Ismach, A. F.; Johnston-Halperin, E.; Kuno, M.; Plashnitsa, V. V.; Robinson, R. D.; Ruoff, R. S.; Salahuddin, S.; Shan, J.; Shi, L.; Spencer, M. G.; Terrones, M.; Windl, W.; Goldberger, J. E. Progress, challenges, and opportunities in two-dimensional materials beyond graphene. *ACS Nano* **2013**, *7*, 2898−2926.
(81) Büchner, C.; Wang, Z.-J.; Burson, K. M.; Willinger, M.-G.; Heyde, M.; Schlögl, R.; Freund, H.-J. A large-area transferable wide band gap 2D silicon dioxide layer. *ACS Nano* **2016**, *10*, 7982−7989.
(82) Novoselov, K. S.; Mishchenko, A.; Carvalho, A.; Castro Neto, A. H. 2D materials and van der Waals heterostructures. *Science* **2016**, *353*, aac9439.

https://doi.org/10.1021/acs.jpcc.1c07311
J. Phys. Chem. C 2021, 125, 23313−23326